Journal of Nuclear Materials 407 (2010) 151–156

Contents lists available at ScienceDirect

Journal of Nuclear Materials

journal homepage: www.elsevier.com/locate/jnucmat

Effects of stress on radiation hardening and microstructural evolution in A533B steel

K. Fujii [a,*], K. Fukuya [a], R. Kasada [b], A. Kimura [b], T. Ohkubo [c]

[a] Institute of Nuclear Safety System, Inc., Mihama-cho, Mikata-gun, Fukui 919-1205, Japan
[b] Institute of Advanced Energy, Kyoto University, Uji 611-0011, Japan
[c] National Institute for Materials Science, Tsukuba, Ibaraki 305-0047, Japan

ARTICLE INFO

Article history:
Received 11 May 2010
Accepted 29 September 2010

ABSTRACT

Bent specimens of A533B steel (0.16 wt% Cu) were irradiated at 290 °C to 1 dpa with 6.4 MeV Fe^{3+} ions. Calculated tensile stresses at the irradiated surface were set to 0, 250, 500 and 750 MPa. The specimens were subjected to hardness measurements, transmission electron microscopy (TEM) observations and three-dimensional atom probe (3DAP) analysis. The radiation-induced hardening decreased with increasing stress to 500 MPa which was near the yield strength. TEM and 3DAP results showed that well-defined dislocation loops and solute clusters were formed. The diameter of dislocation loops increased and the number density decreased when the stress was applied, whereas the diameter and number density of solute clusters decreased. The hardening was mainly attributed to solute cluster formation. Application of tensile stress would control hardening by suppressing the solute cluster nucleation and growth.

1. Introduction

Radiation hardening and embrittlement of reactor vessel steels is known to be sensitive to various material variables and irradiation conditions. Several types of microstructural features have been proposed which are commonly into two groups: solute clusters and matrix damage [1,2]. Many investigations have been carried out to understand the effects of material variables (e.g., Cu content) and irradiation conditions (e.g., neutron flux, temperature) on the hardening and the microstructural evolution. Another parameter which may affect radiation embrittlement is tensile stress since the reactor vessel is also under a tensile stress during operation. However, relatively little attention has been paid to the simultaneous effects of radiation and stress because applied service loadings are relatively low levels such as about 20% of yield strength. Therefore, there have been only a few reports, made in the 1960s, concerning the effects of stress on the ductile to brittle transition temperature (DBTT) shift. The work by Nichols and Harries [3] examined samples pre-strained and then irradiated in the unstressed state. They could not find any effects from stress on the irradiation response of pressure vessel ferritic steels. Reynolds [4] examined A302-B steel irradiated under stress equal to 20% of the yield strength; his results implied that the stress effects led to greater upper shelf energy of the stressed material than the unstressed material. Hawthorne and Loss [5] examined two steels, A350-LF1 forging steel and A302-B plate steel, that were prestressed to 80% of yield strength and then irradiated. No change in irradiation response of both steels was identified, and the results indicated no effects of stress. However, no direct evidence of effects of stress on the evolution of the microstructure in ferritic steels under irradiation has been reported. On the other hand, the effects of stress on the microstructure in neutron irradiated austenitic stainless steels have been investigated to understand void swelling and irradiation creep [6–8]. Studies on the effects of the external stress on the irradiation damage have also been carried out by the techniques of reactor irradiation with a pressurized pipe [7], ultra-high voltage transmission electron microscope irradiation [9,10], light-ion irradiation [11,12] and heavy-ion irradiation [13,14] under tensile stress. All these studies found that applied tensile stress enhanced swelling and creep depending on the microstructural evolutions.

The present study was undertaken to characterize hardening and microstructure evolution in reactor vessel steels under irradiation and stress. Heavy-ion irradiation experiments were carried out for bent specimens of A533B steel. The specimens were examined by hardness measurements, TEM and 3DAP analyses.

2. Experimental procedures

2.1. Specimen preparation and irradiation conditions

Chemical composition of A533B steel used in this study is shown in Table 1. The yield strength at 290 °C is 570 MPa. In the previous studies, it was confirmed that well-defined solute clusters and dislocation loops form in this material under neutron, electron, and heavy-ion irradiations in unstressed condition [15–19].

A specimen holder with the curvature radius of 50 mm was prepared for the irradiation in stressed conditions. The tensile stress

* Corresponding author. Tel.: +81 770 37 9100; fax: +81 770 37 2009.
E-mail address: fujiik@inss.co.jp (K. Fujii).

0022-3115/$ - see front matter © 2010 Elsevier B.V. All rights reserved.
doi:10.1016/j.jnucmat.2010.09.055

Table 1
Chemical composition (wt%).

C	Si	Mn	P	S	Ni	Cr	Mo	Cu	Fe
0.17	0.29	1.45	0.011	0.017	0.55	0.11	0.50	0.16	Balance

(σ) and strain (ε) at the surface in a bending plate were calculated by the following equation,

$$\sigma = \frac{E}{1-v^2}\varepsilon, \quad \varepsilon = \frac{t/2}{\rho}$$

where E is the Young's modulus (=200 GPa), v is the Poisson ratio (=0.33), t is the thickness of the plate, and ρ is the curvature radius at half the plate thickness. The stress and strain at the surface could be controlled by the thickness of the specimens. Specimens measuring 16 × 5 mm were cut out from the sample block. Their thicknesses were adjusted by mechanical and chemical polishing to 0.11, 0.22 and 0.33 mm to get the tensile stress at 250, 500 and 750 MPa and the strain at 1.1×10^{-3}, 2.2×10^{-3} and 3.3×10^{-3} at the surface, respectively. The stress level of 250 and 500 MPa was in elastic condition while the stress level of 750 MPa exceeded the yield strength.

Heavy-ion irradiations were conducted with 6.4 MeV Fe^{3+} ions using the tandem ion accelerator in the Dual-Beam Facility for Energy Science and Technology at Kyoto University [20]. The irradiation temperature was 290 ± 5 °C, which was measured as the surface temperature of the specimens by thermography. The SRIM-2006 code was used for an irradiation damage calculation [21]. The corresponding dose-calculation was done in pure Fe with the displacement energy E_d = 40 eV. The peak damage depth was 1500 nm. The dose and dose rate at a depth of 600 nm were used for damage parameters, since post-irradiation microanalyses were performed at a depth of 600 nm. The applied damage rate and dose were 1.0×10^{-4} dpa/s and 1.0 dpa respectively. The implanted Fe concentration at 600 nm was estimated to be 0.001 at%, which was a negligible level.

2.2. Examinations

Hardness at room temperature was measured using an ultra-micro hardness tester (Elionix ENT1100) with a Berkovich diamond indenter tip. It is known that, in hardness measurement, plastic deformation under an indentation reaches four times as deep as the indentation depth, and that the averaged hardness in such depth was obtained [22]. In the present study, the indentation depth was kept at 300 nm, thus average hardness in the damage region up to about the damage peak depth was measured. The values of hardness were calculated from the maximum load and maximum displacement. The average hardness was determined by averaging over more than 40 indents. The hardness measurements on unirradiated specimens which was annealed at 290 °C for 1×10^4 s in a vacuum under stress of 0, 500 and 750 MPa were also carried out as a reference.

The change of tensile stress due to stress relaxation was measured by X-ray diffraction (XRD) technique before and after irradiation while keeping the specimens in the irradiation holder. The measurements were done using a XRD stress measurement system (Rigaku Model MSF-3 M). Vanadium-filtered Cr Kα radiation of wavelength 0.2291 nm was diffracted from the (2 1 1) planes of iron at 156.4° (2θ), where θ was the Bragg angle. The 2θ-$\sin^2\psi$ method of 10 ψ-angles (0–45°) was used to determine stress at the surface. All the measurements were done at the center of the specimens with a 2 × 2 mm square collimator.

Thin foils for TEM observation were prepared using a focused ion beam (FIB) system (Hitachi FB-2000A) and an ultralow-energy Ar ion beam sputtering system (Technorg-Linda GentleMill IV). Observations were carried out using a TEM (Hitachi HF-3000) equipped with a field emission gun of 300 kV. Analysis of radiation induced defects was carried out at a depth of 600 nm in the specimens using a weak-beam technique; details of this had been described in previously [17].

Needle shaped specimens for 3DAP measurements were prepared using FIB systems (Hitachi FB-2000A and FB-2100). The probe tip was set at the depth of 600 nm. 3DAP measurements were carried out at 60 K using a wide-angled and laser-assisted 3DAP system developed at the National Institute for Materials Science, Japan [23]. An ultraviolet (343 nm) femtosecond (400 fs) laser with pulse energy of 150 nJ/pulse and pulse frequency of 100 kHz was used for atom plobe analysis.

3. Results

3.1. Hardness measurements

Fig. 1 shows results of hardness measurement in the specimens irradiated under different stresses and the unirradiated specimens. The peak position of the hardness distributions in the irradiated specimens shifted to a smaller hardness with increasing stress, whereas that in the unirradiated specimens did not shift. The shape of distribution of hardness did not differ with stress though the distribution of hardness expanded due to irradiation. The average hardness with standard deviation of the irradiated specimens is

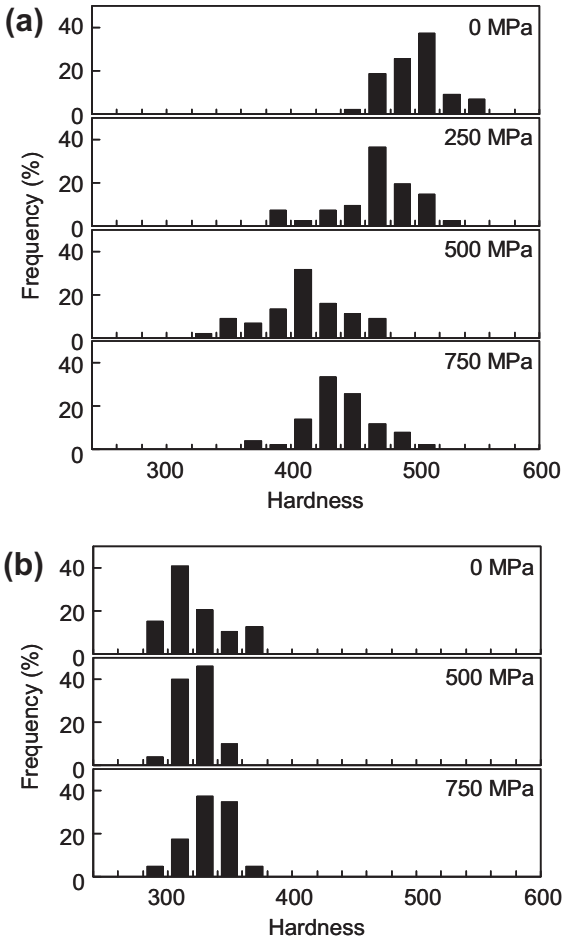

Fig. 1. Hardness measurement results of (a) the specimens irradiated under different stresses and (b) the unirradiated specimens.

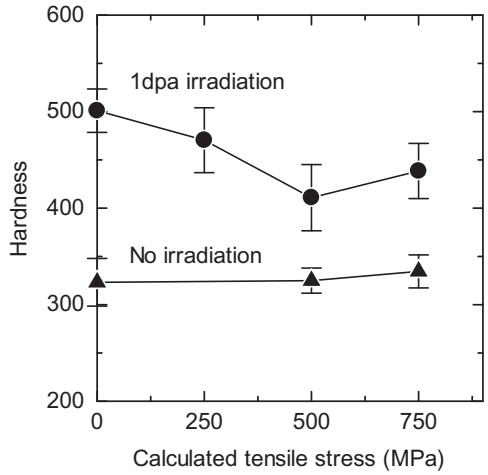

Fig. 2. Effects of tensile stress on irradiation hardening.

plotted against stress in Fig. 2, together with hardness in the specimens annealed under stresses for the same time as the 1 dpa irradiation. The error bars represent standard deviations. The hardness in the irradiated specimens decreased with increasing tensile stress, while the hardness in the annealed specimens remained unchanged. The radiation-induced hardening decreased with increasing stress to 500 MPa, which was near the yield strength. The hardness at 750 MPa was slightly higher than that at 500 MPa in both irradiated and annealed specimens. At 750 MPa the specimens were plastically deformed and had higher hardness than that at 500 MPa even in unirradiated conditions.

3.2. XRD stress measurements

Measured stress by XRD of the bending specimens before and after the irradiation was plotted against the calculated tensile stress in Fig. 3. The error bars indicated the experimental uncertainties for the XRD stress measurements. The data at 250 and 500 MPa lay on the linear relation between the measured stress and the calculated tensile stress. The tensile stress in the specimen under 250 MPa stress slightly increased due to irradiation, whereas the tensile stress in the specimen under 500 MPa stress slightly decreased. However, the change in tensile stress due to irradiation was small. The data at 750 MPa deviated from the linear relation between the measured stress and the calculated tensile stress, because the specimen had deformed plastically. The specimen curved slightly and showed plastic strain after being detached from the irradiation holder. On the other hand, the specimens under 250 and 500 MPa stresses showed no plastic curvature before and after the irradiation.

Some reduction of stress at 500 and 750 MPa indicated that the stress relaxation due to irradiation occurred under the stress levels near and over the yield strength. However, the averaged stress in the region of about 10 μm depth was measured by XRD in the present experimental condition. How the ion irradiation of ~2 μm damage depth contributes to the stress relaxation would require further examination.

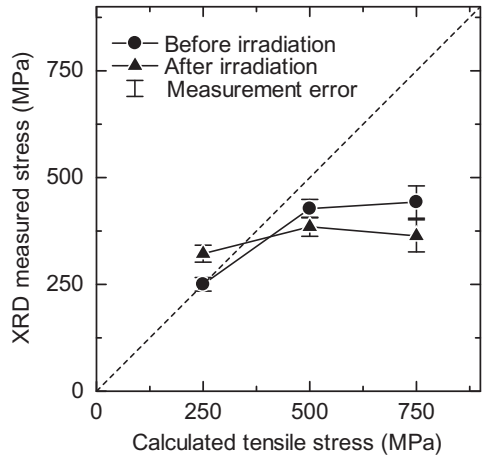

Fig. 3. XRD stress measurement results of bending specimens before and after irradiation.

3.3. TEM observations

Fig. 4 shows bright-field and weak-beam dark-field TEM images in the specimens irradiated without stress and under 500 MPa stress. Black contrasts of irradiation-induced defects were observed in the bright-field images. Small white dots which were dislocation loops were distributed homogeneously over entire area in the weak-beam image. Larger-sized dislocation loops were observed in the specimen irradiated under stress. Weak-beam images of the same area imaged with three kinds of different diffraction vector g in the specimen irradiated under 500 MPa stress is shown in Fig. 5. Dislocation loops in bcc metals show contrast change depending on the Burgers vector $\boldsymbol{b}$ used to image them [24]. Based on the results of the detailed contrast analysis, most of the clearly recognized dislocation loops had $\boldsymbol{b} = a\langle 1\,0\,0\rangle$. The size distribution of the analyzed dislocation loops is shown in Fig. 6. The ratio of large dislocation loops became higher in the specimen irradiated under stress. The average diameter and number density of dislocation loops are shown in Fig. 7. The error bars of the average diameter represent standard deviations and those of the number density indicate the experimental uncertainties for the measurements of the specimen thickness. The number density of disloca-

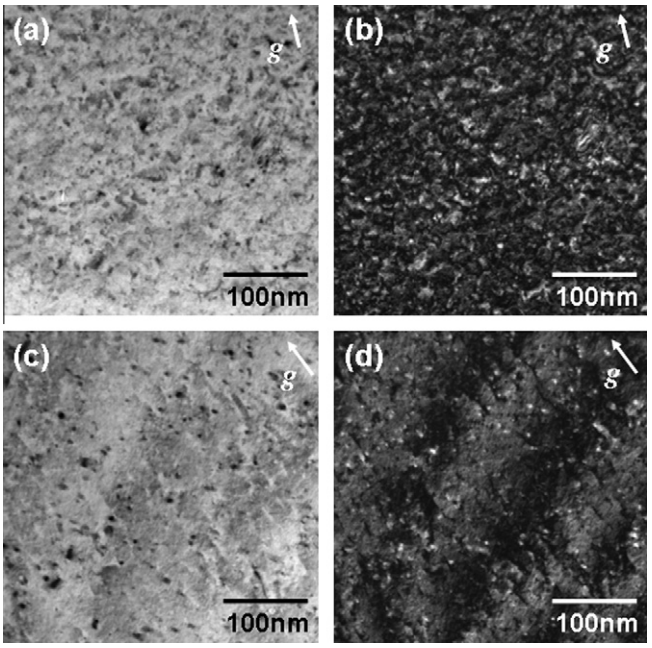

Fig. 4. TEM images. (a and b) Specimen irradiated without stress and (c and d) specimen irradiated under 500 MPa stress. (a and c) Bright-field and (b and d) weak-beam dark-field images imaged with diffraction vector $g = 0\bar{1}1$ close to the [0 1 1] pole.

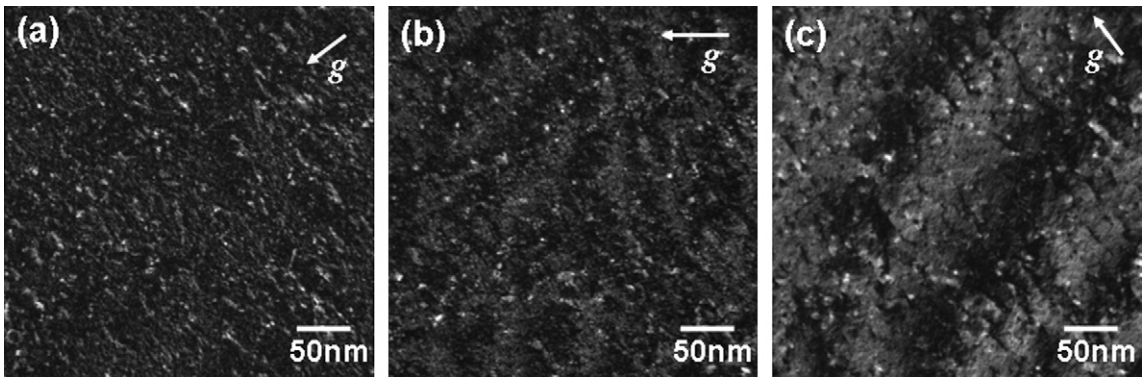

Fig. 5. Weak-beam images of the same area imaged (a) with $g = 200$, (b) $g = 2\bar{1}1$ and (c) $g = 0\bar{1}1$ close to the [0 1 1] pole in the specimen irradiated under 500 MPa stress.

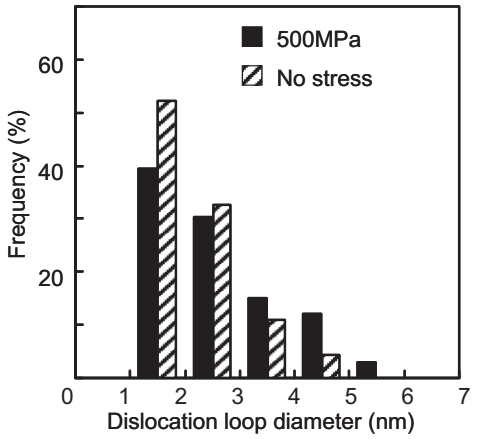

Fig. 6. Size distribution of dislocation loops in the specimens irradiated without stress and under 500 MPa stress.

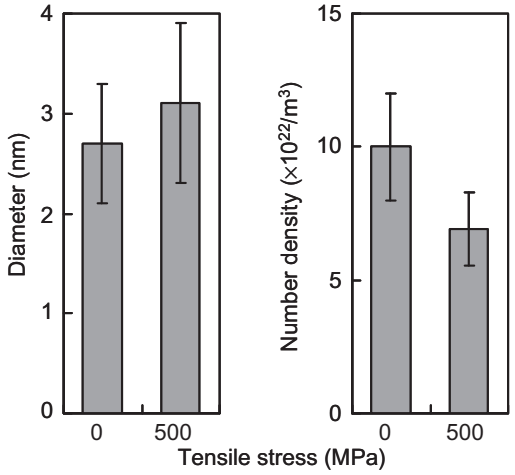

Fig. 7. Diameter and number density of dislocation loops in the specimens irradiated without stress and under 500 MPa stress.

tion loops decreased and the diameter increased when the stress was applied.

3.4. 3DAP measurements

Fig. 8 shows sets of elemental maps in the specimens irradiated without stress and under 500 MPa stress. Elements of mass 58 were used for evaluation of Ni. The clustering of Si, Mn and Ni atoms was clearly observed in both specimens. Although Ga atoms which were used in FIB micro-processing were also detected in these specimens of the elemental maps, the implanted Ga concentration was estimated as 0.1 at%, which was a negligibly low level. In order to obtain quantitative data on the cluster formation, elemental maps were analyzed based on the clustering of Si and Cu atoms which were recognized as the main elements constituting the core of solute clusters in the previous studies [15–19]. The clustering of Si atoms was most clearly observed in both specimens, and the clustering of Mn and Ni atoms was identified in the same position as the Si clustering. Solute clusters would be analyzed by evaluating clustering of Si. Solute clusters were defined as clusters containing more than five Si atoms with Si–Si distances of less than 0.7 nm or containing more than five Cu atoms with Cu–Cu distances of less than 0.7 nm. Under this definition, several Si-core clusters were identified in both specimens whereas no Cu-core clusters were confirmed. The number densities of clusters in the specimens irradiated without stress and under 500 MPa stress were 4.3 and $3.1 \times 10^{24}/m^3$, respectively. The size of clusters was determined using the radius of gyration of clustering atoms. Fig. 9 shows the cluster size distribution. The ratio of small clusters became higher in the specimen irradiated under stress. The average diameter, number density and volume fraction of clusters are shown in Fig. 10. The error bars of the average diameter represent standard deviations, and those of the number density and volume fraction correspond to the scatter in measured values. The size, number density and volume fraction of clusters decreased with stress. The averaged composition of clusters was Fe–4.7Mn–6.3Ni–10.2Si–0.3Cu in the specimens irradiated without stress and Fe–3.3Mn–5.8Ni–11.4Si–0.4Cu in the specimens irradiated under 500 MPa stress. Si–Ni–Mn rich clusters with low Cu content were formed under both conditions. However, the concentration of Si in the clusters under the stressed condition was slightly higher than that under the unstressed condition, whereas the concentrations of Mn and Ni in the cluster under the stressed condition were slightly lower than those under the unstressed condition. Enhancement of Si clustering and suppression of Mn and Ni clustering were suggested under stress.

4. Discussions

Since the reactor vessel is under tensile stress due to inner pressure while undergoing irradiation, the effects of stress on DBTT shift were studied by a few groups as mentioned in introduction. Nichols and Harries [3] and Hawthorne and Loss [5] found no significant effects of stress on DBTT shift. On the other hand, Reynolds [4] found that applied stresses decreased the irradiation-induced

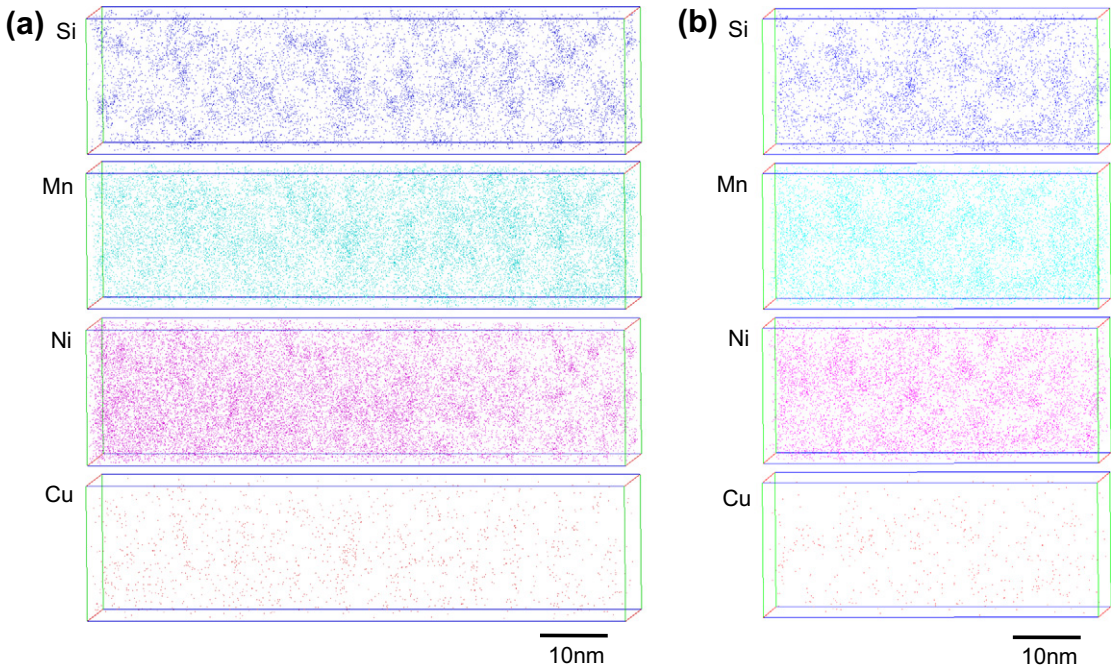

Fig. 8. Atom maps in the specimens irradiated (a) without stress and (b) under 500 MPa stress.

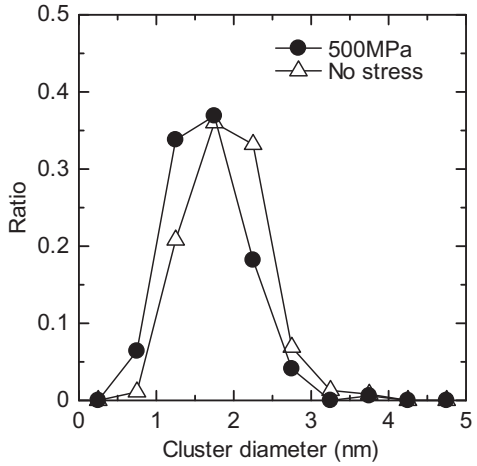

Fig. 9. Size distribution of clusters in the specimens irradiated without stress and under 500 MPa stress.

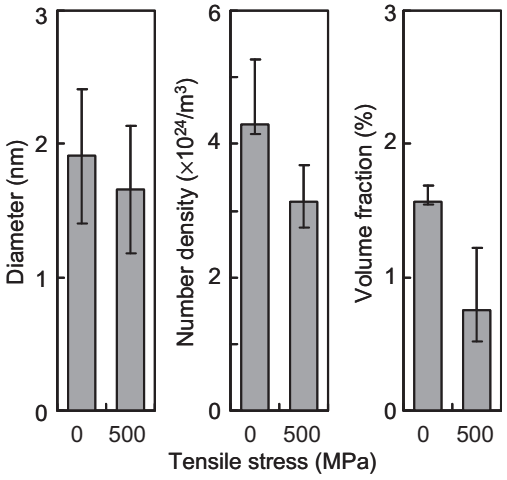

Fig. 10. Diameter, number density and volume fraction of clusters in the specimens irradiated without stress and under 500 MPa stress.

increases in DBTTs. There is a good correlation in the DBTT shift and increase in hardness of reactor vessel steels [25]. The decrease of radiation-induced hardening under the stressed condition found in the present study agreed with the results of DBTT shift obtained by Reynolds [4].

The change of radiation hardening with tensile stresses can be explained by microstructural evolution. Microstructural components identified in the present TEM observations and 3DAP analyses were dislocation loops and solute clusters. These components are known as the main contributors to hardening in low alloy steels. Then, to evaluate the contribution of dislocation loops and solute clusters to hardening quantitatively, the increase in the yield strength due to the formation of dislocation loops and solute clusters was examined by using Orowan's hardening model. In the present experimental condition, the effect of polycrystal on the yield strength increase can be neglected, because the deformation by hardness measurements was limited in a grain. In this case, the yield strength increase is given by $\Delta\sigma = \alpha\mu b\sqrt{N \cdot d}$: where N and d are the number density and diameter of the dislocation loops or solute clusters, μ is the shear modulus (=82 GPa), and b is the Burgers vector (=0.25 nm). α is the hardening efficiency which depends on the nature of a defect. Small loops have relatively small barrier strengths, and the value of 0.2 has been proposed for austenitic steel [26]. In this evaluation the same value was used for α of the dislocation loops. According to the barrier strengths of precipitates, large precipitates have strong barriers and small MC precipitates have intermediate barrier strengths. Though it was thought that the barrier strength of small clusters depended on the composition and size, in this evaluation small clusters would have small barrier strengths and the same value of 0.2 was used for α. The increase of the yield strength due to the dislocation loop formation in the specimens irradiated without stress and under 500 MPa stress were respectively calculated to be 67 MPa and 60 MPa, and those due to the solute cluster formation

were respectively calculated to be 371 MPa and 295 MPa. The hardening was dominated by the solute cluster formation because of its higher number density. The total increases of the yield strength were respectively calculated to be 377 MPa and 301 MPa by using root mean square. The result agreed with the tendency of larger hardening level for the unstressed specimen, and it is likely to explain the effects of stress on radiation hardening by formation of the solute clusters.

The present TEM results suggested that tensile stress suppresses the dislocation loop nucleation and enhances its growth. The effects of stress on the microstructure of neutron irradiated austenitic stainless steels have been investigated and the mechanisms of stress effect, such as stress-induced preferential attraction (SIPA) of point defects [27] and stress-induced preferential loop nucleation (SIPN) [28], were proposed. These mechanisms mainly targeted the microstructural evolution of dislocation loops. In the present study, though the dislocation loops were observed as irradiation-induced defects, the anisotropy of dislocation loop formation could not be examined, because the observed dislocation loops were too small to decide their Burgers vectors and the decision of the relation between the Burgers vector of each dislocation loops and the stress axis was very difficult. Therefore, the effects of stress on the observed dislocation loops could not be discussed directly for the SIPA and/or SIPN mechanisms. However the obtained tendency that stress reduced the number density of dislocation loops and increased their size corresponded to dislocation loop evolution under irradiation at higher temperature conditions.

The present 3DAP results suggested that tensile stress affects irradiation hardening by suppressing the cluster nucleation and growth. Though the mechanism for the effects of stress on the solute cluster formation and growth is not clear, suppression of the solute cluster nucleation and growth under stress would correspond to accelerated diffusion of point defects into perfect sinks and to lowered effective point-defect concentration. Based on the assumption that dislocation loops act as the nucleus of Mn–Ni–Si cluster, the decrease of the number density of dislocation loops might affect to the decrease of the number density of solute clusters. Moreover, the result that the Si concentration was higher and the Mn and Ni concentrations were lower in the clusters formed under the stressed condition suggests the possibility that the effect of vacancies on clustering was suppressed by the stress and/or the effect of interstitials on clustering was promoted by the stress if Si clustering corresponds to interstitials. In addition, it has been reported that stress mitigated irradiation induced segregation of solutes in austenitic stainless steels [14], and the results related to the suppression of the solute clustering and the cluster growth under stress. However further experimental efforts are needed to fully understand the effects of stress.

5. Conclusions

To characterize the effects of stress on hardening and microstructural evolution in reactor vessel steels, heavy-ion irradiation experiments were carried out on bent specimens of A533B steel. The radiation-induced hardening decreased with increasing stress to 500 MPa which was near the yield strength. TEM and 3DAP results showed that well-defined dislocation loops and solute clusters were formed. The diameter of dislocation loops increased and the number density decreased when the stress was applied. The diameter and number density of solute clusters decreased. The hardening was mainly attributed to solute cluster formation. Application of tensile stress would control hardening by suppressing the solute cluster nucleation and growth.

Acknowledgements

A part of this study was financially supported by the Budget for Nuclear Research of the Ministry of Education, Culture, Sports, Science and Technology (MEXT), based on the screening and counseling by the Atomic Energy Commission. Heavy-ion irradiations were served by the MEXT supported program "Open Advanced Facilities to Industry", named Project ADMIRE (Application of DuET and MUSTER for Industrial Research and Engineering). The authors thank Dr Sosuke Kondo, Mr Okinobu Hashitomi and Mr Kiyohiro Yabuuchi for their support of heavy-ion irradiations.

References

[1] S.B. Fisher, J.E. Harbottle, N. Aldridge, Philos. Trans. Roy. Soc. A 315 (1985) 301.
[2] G.R. Odette, G.E. Lucas, Radiat. Eff. Def. Solids 144 (1998) 189.
[3] R.W. Nichols, D.R. Harries, Symposium on Radiation Effects and Neutron Dosimetry, ASTM STP 341, 1963, p. 162.
[4] M.B. Reynolds, Mater. Res. Stand. 3 (1963) 644.
[5] J.R. Hawthorne, F.J. Loss, Nucl. Eng. Des. 8 (1968) 108.
[6] H.R. Brager, F.A. Garner, G.L. Guthrie, J. Nucl. Mater. 66 (1977) 301.
[7] D.L. Porter, M.L. Takata, E.L. Wood, J. Nucl. Mater. 116 (1983) 272.
[8] F.A. Garner, D.S. Gelles, J. Nucl. Mater. 159 (1988) 286.
[9] D.R. Okamoto, S.D. Harkness, J. Nucl. Mater. 48 (1973) 204.
[10] N. Igata, Y. Kohno, J. Nishimura, J. Nucl. Mater. 149–143 (1986) 790.
[11] H.K. Sahu, P. Jung, J. Nucl. Mater. 136 (1985) 154.
[12] J. Nagakawa, H. Shiraishi, M. Okada, H. Kamitsubo, I. Kohno, T. Shikata, J. Nucl. Mater. 133–134 (1985) 497.
[13] H. Tanigawa, A. Kohyama, in: Proc. 3rd Sino-Japanese Symp. on Materials for Advanced Energy Systems and Fission and Fusion Eng., Chengdu, China, 1995.
[14] K. Kondo, Y. Miwa, N. Okubo, Y. Kaji, T. Tsukada, in: Proc. 13th Int. Conf. on Environmental Degradation of Materials in Nuclear Power Systems – Water Reactors, CNS, 2007.
[15] K. Fukuya, K. Ohno, H. Nakata, S. Dumbill, J.M. Hyde, J. Nucl. Mater. 312 (2003) 163.
[16] K. Fujii, K. Fukuya, H. Nakata, K. Hono, Y. Nagai, M. Hasegawa, J. Nucl. Mater. 340 (2005) 247.
[17] K. Fujii, K. Fukuya, J. Nucl. Mater. 336 (2005) 323.
[18] K. Fujii, H. Nakata, K. Fukuya, T. Ohkubo, K. Hono, Y. Nagai, M. Hasegawa, T. Yoshiie, J. Nucl. Mater. 400 (2010) 46.
[19] K. Fujii, K. Fukuya, T. Ohkubo, J. Nucl. Mater., in press.
[20] A. Kohyama, Y. Katoh, M. Ando, K. Jimbo, Fusion Eng. Des. 51–52 (2000) 789.
[21] J.F. Ziegler, J.P. Biersak, Stopping and Range of Ion in Materials (SRIM), 2006.
[22] Y. Katoh, T. Muroga, T. Iwai, O. Motojima, J. Jpn. Inst. Metals 61 (1997) 191.
[23] Y.M. Chen, T. Ohkubo, M. Kodzuka, K. Morita, K. Hono, Scripta Mater. 61 (2009) 693.
[24] B.L. Eyre, D.M. Maher, R.C. Perrin, J. Phys. F: Metal Phys. 7 (1977) 1371.
[25] G.R. Odette, P.M. Lomborzo, R.A. Wullaert, ASTM STP 870, 1985, p. 840.
[26] N. Yoshida, J. Nucl. Mater. 174 (1990) 220.
[27] P.T. Heald, M.V. Speight, Philos. Mag. 29 (1974) 1075.
[28] W.G. Wolfer, J.P. Foster, F.A. Garner, Nucl. Technol. 16 (1972) 55.